RSC Advances

ROYAL SOCIETY OF CHEMISTRY

www.rsc.org/advances

ARTICLE TYPE

Reduced graphene oxide as a high efficient adsorbent for 1-naphthol and the mechanism thereof

Mohamed Mukthar Ali and K. Y. Sandhya[*]

Herein, adsorption and removal of 1-naphthol from water using reduced graphene oxide (rGO) is reported. The adsorption isotherms of dissimilar rGOs at different temperatures (303 and 323 K) fit well with Langmuir adsorption isotherm. At 303 K, the maximum adsorption capacities (q_{max}) of the relatively lower and higher surface area rGOs (l-rGO and h-rGO) are 3.57 and 5.55 mmol g^{-1} respectively. The q_{max}
10 for the adsorption of 1-naphthol by h-rGO, at 323 K, is a remarkable 8.6 mmol g^{-1}, which is the highest so far reported in the literature.The q_{max} value is greater than that of water dispersible graphene counterpart reported in literature.Acidic and alkaline pH increases the adsorption. Examination of the adsorption mixture using atomic force microscopy proves that the rGOis dispersed as few layered graphene nanosheets. The remarkably higher q_{max} of rGO is attributed to the higher surface area of rGO in aqueous
15 solution due to its exfoliation by 1-naphthol. In summary, rGO is a promising material for the removal of 1-naphthol from water and our findings help in better understanding the mechanism of the adsorption of 1-naphthol and similar compounds by rGO.

1. Introduction

Dissolved organic matters in wastewater are a major concern for
20 health, environment and ecosystem. Textile, leather, paper, printing, plastic industries etc use various chemicals, most of them, aromatic in nature. Due to their non-degradability, aromatic compounds are persistent pollutants and removal of them from wastewater remains a challenge for industries. Aromatic
25 compounds in wastewater cause damage to many forms of life. Potential carcinogenicity of aromatic hydrocarbons and their derivatives emphasize the importance of their removal from the aqueous system. Different techniques such as photodegradation [1] sonochemical degradation [2], coagulation [3], biodegradation
30 [4] and adsorption [5] etc are employed to remove the pollutants. From these methods, adsorption is the most popular one because of its cost-effectiveness, simplicity, efficiency, fastness and due to the fact that it does not lead to the formation of harmful secondary products.
35 Activated carbon powder is a well-known adsorbent which has been widely studied and applied due to its high adsorption capabilities [6, 7]. Recently, carbon nanomaterials such as carbon nanotubes (CNT) [8] and graphene [9, 10] are attracting the attention in the management of aromatic pollutants due to their
40 aromatic benzene rings and higher specific surface areas (SA) which facilitates the adsorption of aromatic compounds efficiently. Graphene due to its exceptionally high theoretical SA (~2600 m^{2}g^{-1}) and cost effectiveness is receiving greater attention from research community as an adsorbent. Li et al used few-
45 layered graphene nanosheets made by ultrasonication of a 1-

methyl-2-pyrrolidinone (NMP) suspension, for the adsorption of fluoride from aqueous solutions achieving an adsorption capacity of 35 mg g^{-1} [11]. Functionalized/modified graphene is used for removal of heavy metal ions such as Pb^{2+}, Cd^{2+} [12] and Cr^{6+}
50 [13]. Adsorption and removal of dyes such as methyl orange, methylene blue, rhodamine B, etc. [14,15] from aqueous solutions using chemically exfoliated reduced graphene oxide (rGO) [16, 17]are investigated. Pei et al [18] reported the adsorption characteristics of naphthalene based aromatic effluents
55 with different functional groups on GO and rGO. Removal of gaseous pollutants such as NO$_x$, SO$_x$ and CO etc., inorganic cations, anions and organic dyes from environment are investigated using graphene materials [19].Aggregation of graphene in aqueous solution is a major issue which reduces the
60 adsorption efficiency of rGO. Therefore, for better performance, water dispersible (modified) graphene materials [20] are investigated as adsorbents for removal of pollutants. In accordance, an aqueous dispersible sulphonated graphene material which forms few layer graphene nanosheets in water
65 exhibits the highest maximum adsorption capacity (q_{max}) for aromatic compounds such as naphthalene and 1-naphthol [9, 21]. 1-naphthol is an aromatic pollutants present in the environmental system which acts as precursor for insecticides and dyes. It causes hemolysis, nephritis, irritation to respiratory organs and
70 skin and is a potential carcinogenic agent. Iron oxide modified graphene material (iron oxide-rGO) [10] was reported to have an efficiency of 1.68 mmol g^{-1}. However, none of these reports investigated the adsorption of 1-naphthol using (unmodified) rGO.

In this paper, we show that rGO has the highest adsorption efficiency for 1-naphthol, higher than the water dispersible counterpart reported in the literature. We conducted the adsorption experiment with two different rGOs, a relatively lower SA rGO (l-rGO) and higher SA rGO (h-rGO) and at different temperatures (303 and 323 K). The q_{max} values at 303 K of l-rGO and h-rGO are 3.57 mmol g^{-1} (515 mg g^{-1}) and 5.55 mmol g^{-1} (800 mg g^{-1}), respectively. At 323 K, the q_{max} value is a remarkable 8.6 mmol g^{-1}(1241.8 mg g^{-1}) for h-rGO, evidently the highest value so far reported for 1-naphthol. Analysis of the adsorption mixture using atomic force microscopy (AFM) reveals that 1-naphthol disperses rGO as nanosheets of ≤10 nm thickness. The results show that rGO is a super adsorbent material for 1-naphthol and suggest that it may act as a highly efficient adsorbent for similar aromatic compounds, which are capable of dispersing rGO in aqueous solutions. The adsorption efficiency may depend on the structure of the adsorbate, the number of benzene rings and other factors.

2. Experimental

2.1 Raw materials

Graphite (21 μm) was purchased from Sigma Aldrich India Co. Ltd. Intercalated graphite (IC) was purchased from Anthracite industries. Potassium permanganate (99%), hydrogen peroxide (30%), hydrochloric acid (35%), sulfuric acid (98%) and 1-naphthol (99% of reagent grade) were purchased from Merck, India Ltd. Distilled water was usedfor all the experiments.

2.2 Preparation of GO

Two different methods were used to prepare GO, in the attempt to make different SA rGOs. The GOs used for preparing comparatively lower and higher SA rGOs were represented as l-GO and h-GO, respectively. Preparation procedure of l-GO (modified Hummer's method) was described elsewhere [22].

l-GO was synthesized by reacting commercial graphite powder with H_2SO_4 and $KMnO_4$ followed by addition of H_2O_2. The solid brown product was filtered and washed repeatedly with 1 M HCl and then with distilled water and finally dried under vacuum at room temperature.

For h-GO preparation, IC was used in the place of graphite. IC was thermally expanded by heating at 1050 °C for 30 seconds under argon atmosphere [23] to produce the thermally expanded graphite (TEG). In a typical reaction, 2 g of TEG was mixed with 240 mL of con.H_2SO_4 in a three neck RB flask. The flask was kept in an ice bath and then 16 g of $KMnO_4$ were slowly added under stirring and the mixture was stirred at 90 °C for 24 h. Then the mixture was cooled to room temperature and 400 mL of water were added, followed by the slow addition of 50 mL of H_2O_2 till the color of the suspension turned to light brown. The product was washed with HCl solution three times and plenty of water to bring the down the pH to 5. The suspension was then centrifuged and the product was dried under vacuum at 70 °C overnight.

2.3 Preparation of rGO

In a typical procedure [24] 200 mg of GO and 200 mL water were introduced in a three neck flask and sonicated to yield a homogeneous yellow brown dispersion. To the homogenous solution 2 mL of hydrazine hydrate were added and the resultant solution was refluxed at 100 °C under a water cooled condenser for 24 h. The rGO gradually precipitated out as a black solid. The product was filtered off and washed with water and methanol and then dried at 60 °C under vacuum overnight. l-GO and h-GO after reduction yields l- rGO and h-rGO, respectively.

2.4 Characterization

Perkin Elmer spectrum100 Fourier transform infra-red (FTIR) spectrophotometer was used for recording IR spectra. X-ray diffraction (XRD) patterns were obtained using Xpert-pro diffractometer with K_α wavelength (1.54 Å) of Cu metal. Thermogravimetric Analysis (TGA) was done using TA Q50. Absorption spectra were recorded using CARY 100 Bio UV-Vis spectrophotometer. Brunauer-Emmett-Teller (BET) SA analyses were done using Tristar II micromeritics SA analyzer. Degasification of the samples for SA analyses were done at 120 °C for 8 h, prior to nitrogen (N_2) adsorption isotherm. N_2 adsorption isotherms were carried out at 77 K using liquid N_2 as a coolant. p/p_0 values in the range of 0.05 to 0.25 were used for calculating the BET SA values. Raman spectral analyses were carried out using WiTech alpha 300R with 532 nm excitation laser. AFM analyses were carried out in Agilent 5500 scanning probe microscope.

2.5 Adsorption studies

For adsorption studies, 5.26 mmol $L^{-1}$of 1-naphthol solution was used as stock solution. For the contact time studies, 0.1 mg mL^{-1} of rGO in water and 1mmol L^{-1} of 1-naphthol solution were used. Effect of pH experiments were carried out using 1 mmol L^{-1} 1-naphthol solutions. For adsorption isotherm studies, 0.1 mg mL^{-1} of rGO in water was used. All adsorption studies were done using a 20 mL sample tube with a working volume of 8 mL. Agitation was provided with a mechanical hand-shaker in dark conditions. Adsorbent was removed from the mixture by centrifugation and the supernatant was analysed using UV-Vis spectrophotometer. Absorbance value at 290 nm was used for determining the 1-naphthol concentration.

3. Results and Discussion

Figure 1 provides the FTIR spectra, thermograms, N_2 adsorption-desorption isotherms and Raman spectra of the l-GO and l-rGO. The formation of rGO is explained using the results of l-GO and l-rGO. The IR spectrum of l- GO (Figure 1A) displays peaks at 3400 and 1640 cm^{-1} corresponding to the stretching and bending of hydroxyl (-OH) groups, peaks at 1718 and 1623 cm^{-1} are due to –C=O and skeletal -C=C- stretching vibrations, respectively. Epoxy C-O-C stretching peak is observed at 1223 cm^{-1}.No peaks are observed in the IR spectrum of l-rGO indicating reduction of GO to rGO. The thermogram of l-GO shows two-step weight loss, around 100 and 200 °C and are attributed to the loss of water molecules and the removal of oxygen functional groups from GO respectively. The residual mass for l-GO at 750 °C is 35 % and that of the rGO is ~85 %. The weight loss in l-rGO is attributed to the removal of edge functional groups. The results confirm the formation of rGO.

The results of BET SA analyses and N_2 adsorption−desorption isotherms of l-GO and l-rGO are shown in Figure 1C. The comparatively lower SA of GO (24 $m^2 g^{-1}$) is assigned to the
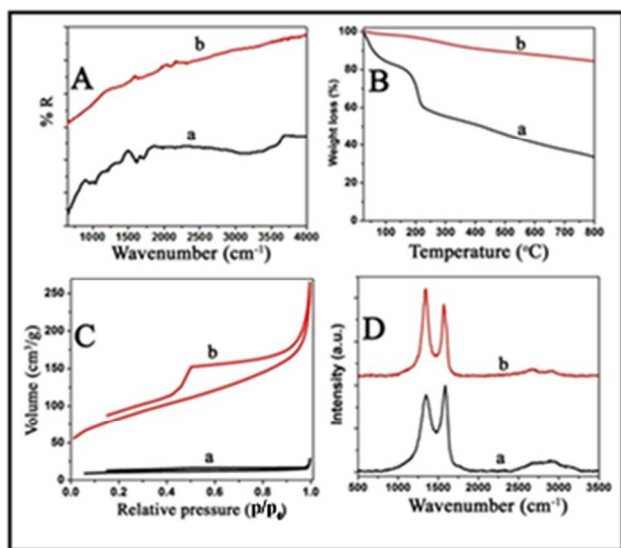
Figure 1. (A): FTIR spectra; (B): TGA spectra; (C): N$_2$ adsorption-desorption isotherms and (D): Raman spectra of (a): l-GO and (b): l-rGO

interactions of the functional groups which lead to the stacking of layers. In rGO due to the removal of functional groups, the rGO layers assume a random aggregation of graphene layers by the weak π-π interactions and edge functional groups leading to higher SA. The N$_2$ adsorption−desorption isotherms and the SA values of l-rGO and h-rGO are given in Figure S1[§] and Table S1[§], respectively.The SAs of l-rGO and h-rGO are 287 and 418 m^2 g^{-1}, and the pore sizes are 4.8 and 2.7 nm, respectively. The Raman spectra of GO and rGO show the D (due to defect) and G (graphitic) peaks at 1360 and 1580 cm^{-1} and I$_D$/I$_G$ ratio of rGO shows an increase which agrees with the earlier report [24]. Thus, the characterization results confirm the formation of different SA rGOs.

3.1 Adsorption of 1-naphthol by the rGOs:

It is observed that the adsorption of 1-naphthol by l-rGO reaches equilibrium quicker than that of h-rGO (Figure S2)[§]. The h-rGO reaches the equilibrium in ~50 h while l-rGO reaches much earlier. Kinetic parameters are given in Table S2[§] and shows that the adsorption of 1-rGO fits with pseudo first order while that of the h-rGO fits with pseudo second order kinetics (supplementary info).This difference is attributed to the difference in their pore sizes (Table S1[§]). In accordance to an earlier study [9], 5 days of time is used in our adsorption experiments. The amount of 1-naphthol adsorption at equilibrium is calculated using the following equation,

$$q_e = \frac{(C_0 - C_e)*V}{m} \quad (1)$$

Where q_e is the quantity of 1-naphthol adsorbed over rGO (mmol g^{-1}), C_0 and C_e are the initial and equilibrium concentrations of 1-naphthol in aqueous solution (mmol L^{-1}), V is the volume of the solution (L), and m is the mass of the adsorbent (g).

The adsorption isotherms provide the details of interaction between adsorbate and adsorbent at equilibrium. The linear form of Langmuir adsorption isotherm [25] can be expressed as:

$$\frac{C_e}{q_e} = \left(\frac{1}{bq_0}\right) + \left(\frac{1}{q_0}\right)C_e \quad (2)$$

Where C_e and q_e are equilibrium concentration of 1-naphthol (mmol L^{-1}) in solution and the amount of 1-naphthol adsorbed on rGO (mmol g^{-1}) respectively. The q_0 and b are the Langmuir constants related to adsorption capacity and affinity of binding sites respectively [26]. Plotting C_e against C_e/q_e will give the q_0 and b values. The Freundlich model of adsorption [27] assumes multilayer adsorption on a heterogeneous surface. The linear form can be expressed as:

$$\log q_e = \log K_f + \left(\frac{1}{n}\right)\log C_e \quad (3)$$

K_f and n are Freundlich constants where K_f(mmol^{1-n} g^{-1} L^n) and n give an idea of the adsorption capacity of the adsorbent and how favourable the adsorption process is, respectively. The adsorption isotherms and the linear fit models of adsorption isotherms for the adsorption of 1-naphthol by the rGOs and the parameters of adsorption isotherms are given in Figure 2 and Table 1, respectively. The relative coefficient (R^2) values suggest that the Langmuir model of adsorption fits well for the adsorption of 1-naphthol by the rGOs. Langmuir model assumes the adsorption is of monolayer, the surface of adsorption is homogenous in nature and there is no chemical interaction between the adsorbed species. To find out the reversible nature of the adsorption process, Langmuir isotherm can provide the dimensionless parameter (R$_L$) [28] and can be expressed as:

$$R_L = \left(\frac{1}{1+bC_0}\right) \quad (4)$$

Where b is a constant and C_0 is the highest initial 1-naphthol concentration (mmol L^{-1}).The experimental R$_L$ values obtained for l-rGO and h-rGO are 0.11 and 0.026, respectively. The R$_L$ values are between 0 and 1 (0<R$_L$<1), which essentially imply that this type of adsorption isotherm is favourable in both the cases [29].
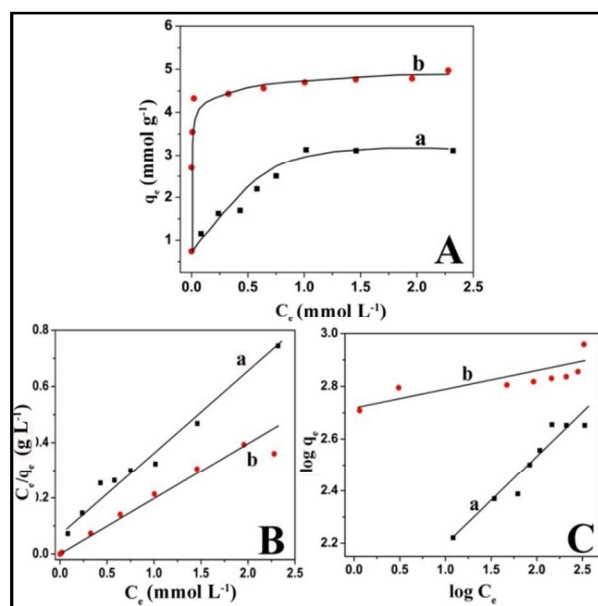
Figure 2.(A): Adsorption isotherms (A) and linear fits of Langmuir and Freundlich adsorption isotherms for the adsorption of 1-naphthol (B and C): by (a) l-rGO and (b) h-rGO at 303 K, respectively. Initial concentrations of 1-naphthol are 0.1-3 mmol L^{-1}and rGO is 0.1 mg mL^{-1}

ARTICLE TYPE

Table 1. Adsorption parameters obtained from the isotherms for the adsorption of 1-naphthol by l-rGO and h-rGO at 303 K

Adsorbent	Parameters	l-rGO at 303 K	h-rGO at 303 K
Langmuir Adsorption model	q_0 (mmol g^{-1})	3.574	5.552
	b (L mmol^{-1})	3.432	16.46
	R^2	0.9746	0.9663
Freundlich Adsorption model	(1/n)	0.338	0.061
	K_f (mmol^{1-n} g^{-1} L^n)	0.49	3.66
	R^2	0.91484	0.601

The maximum adsorption capacity (q_{max}) obtained for the adsorption of 1-naphthol by l-rGO and h-rGO at 303 K, are 3.57
5 and 5.56 mmol g^{-1} (515.46 and 800.7 mg g^{-1}), respectively. The values are significantly higher than the q_{max} of water dispersible sulphonated graphene material (2.3- 2.5 mmol g^{-1}) with a similar SA (387 m^2 g^{-1}) [9], iron oxide modified rGO (rGO-iron oxide) (1.686 mmol g^{-1}) [10], carbon nanotube (0.377 mmol g^{-1}) [30]
10 and many other adsorbents in the literature. For comparison, the q_{max} values of various adsorbents reported in the literature and our values are compiled in Table 2.The values clearly indicate that rGO has the highest adsorption efficiency for 1-naphthol compared to that of the other adsorbents. The comparatively
15 lower value of rGO-iron oxide to that of the rGO may be due to the presence of iron oxide on graphene sheets which might limit the SA available for 1-naphthol adsorption by π-π interaction. It must be highlighted that the adsorption capacity exhibited by rGO is higher than its water dispersible sulphonated graphene
20 counterpart. However, the highest value reported for the adsorption of 1-naphthol is 6.4 mmol g^{-1} [21] at 333 K by the water dispersible sulphonated graphene. Also rGO-iron oxide exhibits an increase from 1.686 mmol g^{-1} at 303 K to a 4.03 mmol g^{-1} at 323 K. Hence we conducted adsorption experiments
25 at higher temperature.

Table 2. The q_{max} values of various adsorbents reported in the literature for the adsorption of 1-naphthol at 303 K in comparison to our results

S. No.	Adsorbent	q_{max} (mmol g^{-1})	References
1	l-rGO	3.57	Our result
2	h-rGO	5.55	Our result
2	Sulfonated graphene	2.4	[9]
3	GO-iron oxide	1.584	[10]
4	rGO-iron oxide	1.686	[10]
5	MWCNT	0.377	[30]
6	Oxidized MWCNT	0.212	[30]
7	Bentonite	0.128	[31]

3.2 Adsorption at higher temperature:

30 Previous reports of 1-naphthol by graphene materials demonstrate that the adsorption is endothermic in nature. We conducted the adsorption experiments at higher temperature (323 K) using h-rGO. The h-rGO was chosen for higher temperature studies because of its higher q_{max} value compared to that of the l-rGO and
35 in addition its SA is similar to that of the sulphonated graphene. The adsorption isotherms and the parameters obtained at higher temperature experiments are given in Figure 3 and Table 3, respectively. In accordance with room temperature results, the Langmuir adsorption isotherm fits better than the Freundlich
40 isotherm. The q_{max} value at 323 K is a remarkable 8.6 mmol g^{-1} and is the highest value reported for the adsorption of 1-naphthol. The result clearly indicates that rGO is an excellent nanomaterial for the adsorption and removal of 1-naphthol from aqueous solutions. In an attempt to find the rationale for the remarkably
45 higher value of rGO we further conducted experiments and analyses using the adsorption mixture.
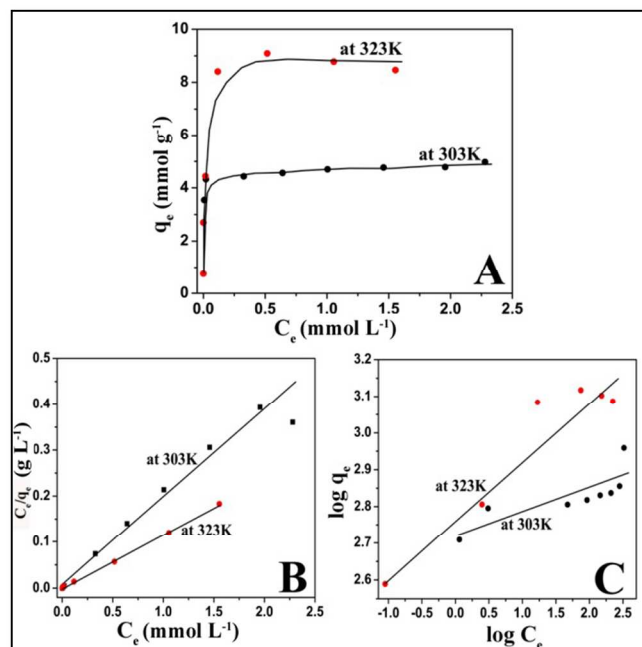

Figure 3.(A): Adsorption isotherms of h-rGO at 303 and 323 K; (B and
50 C): Langmuir and Freundlich linear fit adsorption isotherms at 303 K and 323 K. The initial 1-naphthol concentrations are 0.1-3 mmol L^{-1} and rGO is 0.1 mg mL^{-1}

3.3 Mechanism of adsorption of 1-naphthol by rGO and the structure of 1-naphthol adsorbed rGO (rGO-naphthol):

55 It is well known that rGO, due to its hydrophobic nature, is not dispersible in water. We observed that the initially aggregated rGO in the adsorption mixture during adsorption forms a stable dispersion. The digital photoimages of the dispersions of h-rGO at 323 K and l-rGO at 303 K are given in Figure 4A§ and Figure

RSC Advances Accepted Manuscript

S3[§], respectively. The images evidently show that 1-naphthol disperses rGO in water and the dispersion of rGO in water

Table 3. Adsorption parameters obtained from the isotherms for the adsorption of 1-naphthol by h-rGO at 303 and 323 K

Adsorbent	Parameters	h-rGO at 303 K	h-rGO at 323 K
Langmuir Adsorption model	q_0 (mmol g^{-1})	5.55	8.61
	b (L mmol^{-1})	16.46	689
	R^2	0.9663	0.9993
Freundlich Adsorption model	(1/n)	0.061	0.160
	K_f (mmol^{1-n} g^{-1} L^n)	3.66	4.15
	R^2	0.601	0.8922

increases with the concentration of 1-naphthol. The digital photoimages of the adsorption mixture of h-rGO and 1 mmol L^{-1} of 1-naphthol at 303 and 323 K given in Figure 4B demonstrate that the dispersion of rGO increases with increasing temperature. The exfoliation of rGO can be initiated by the sliding mechanism of 1-naphthol into the graphene layers due to $\pi-\pi$ interactions. The exfoliated graphene layers are well stabilized by the π-π interaction between rGO and 1-naphthol and the interaction of -OH groups of 1-naphthol with water molecules. The dispersion of rGO in water as few layered graphene nanosheets will result in an increase in the SA of rGO, which in turn increases the adsorption capacity of rGO. Dispersion of graphene sheets in aqueous solutions by pyrene derivatives [32-34] is been reported. Very recently Kim et al [35] reported the exfoliation of graphite in various organic solvents by ultrasonicating in presence of naphthalene and achieved graphene concentration of 0.15 mg mL^{-1} in NMP solvent using this procedure. The report mentions that the naphthalene adsorbed over graphene layers acts as a molecular wedge and exfoliates graphite. To the best of our knowledge, this is a first report of a naphthalene moiety dispersing and stabilizing graphene nanosheets in aqueous solution. The sulphonated graphene material dispersed as few layered nanosheets exhibits comparatively lower q_{max} value. Therefore, we assume that rGO is dispersed as few layered graphene nanosheets comprising of bi, tri- layers *etc*. in water. The comparatively lower q_{max} of water dispersible sulphonated graphene may be due to the presence of bulky sulphonated groups which may hinder the adsorption of 1-naphthol.

In the attempt to prove our assumptions, we further characterized the dispersions and dry rGO-naphthol samples using XRD, TGA and AFM techniques. The XRD patterns (Figure 4C) of h-rGO-naphthol show a sharp peak at 20.1° and the broad characteristic peak of rGO at 26.5° while that of the rGO shows only the broad peak around 26.5°. The broad peak centered on 26.5° is due to the typical (002) random ordering of graphene sheets with an interlayer spacing of 0.36 nm. The peak at 20.1° in the rGO-naphthol is sharp and corresponds to an interlayer spacing of ~0.44 nm. This increased spacing is attributed to the 1-naphthol adsorbed rGO layers. The presence of two peaks (20.1° and 26.5°) in the XRD spectrum indicates that the rGO-naphthol has the typical (002) random ordering of graphene sheets and the higher spacing due to the 1-naphthol adsorbed graphene sheets. The thermograms of l-rGO, 1-naphthol and l-rGO-naphthol with

different 1-naphthol content are provided in Figure S3[§]. The thermograms confirm the presence of 1-naphthol in the rGO-naphthol and suggest that the 1-naphthol molecules are trapped in between the rGO layers due to which the sublimation of 1-naphthol becomes unfavorable.

Height profile of the AFM images (Figure 4D) reveal graphene nanosheets of thickness between 1-8 nm, (Additional AFM image with height profiles is given in Figure S4[§]). The images evidently support the formation of graphene nanosheets in water by 1-naphthol. Our results show that 1-naphthol can disperse and stabilize rGO as graphene nanosheets in water, which in turn enhances the adsorption efficiency. The finding also suggests that similar aromatic compounds with appropriate groups can disperse rGO to graphene nanosheets in water and the adsorption efficiency of rGO for such compounds may possibly be high and depends on the number of benzene rings, its structure and other factors. A schematic of the mechanism of dispersion of rGO by 1-naphthol is depicted in Figure 5 and illustrates the exfoliation of graphene into few layered nanosheets in water due to the adsorption of 1-naphthol.
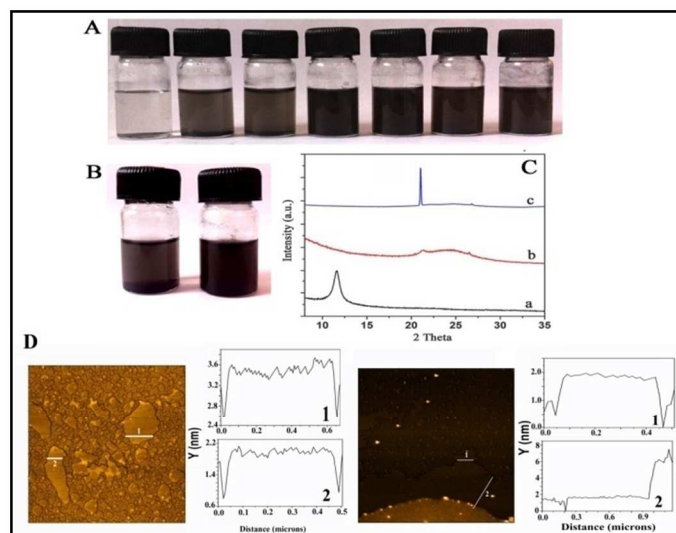

Figure 4. (A): Digital images of h-rGO dispersions (0.1 mg mL^{-1}) in presence of different concentrations of 1-naphthol after 5 days of stirring at 50 °C. From L to R, initial 1-naphthol concentrations are 0.1, 0.3, 0.5, 1, 1.5, 2 and 3 mmol L^{-1}, respectively. (B): Digital images of h-rGO dispersions (0.1 mg mL^{-1}) in presence of 1 mmol L^{-1} of 1-naphthol (L to R): at 303 and 323 K, respectively; (C): XRD of dried samples of (a) h-GO; (b) h-rGO and (c) h-rGO-naphthol (D): AFM images of h-rGO-naphthol dispersion drop-casted on to mica sheets. The AFM images show graphenenanosheets of thickness from 1-8 nm due to the exfoliation of rGO by 1-naphthol in water.
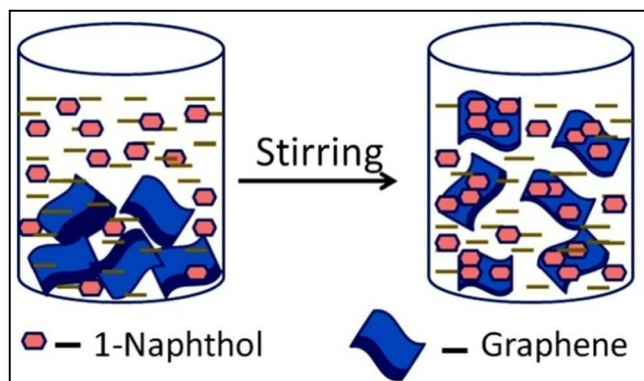
Figure 5.Illustration of the mechanism of dispersion of rGO to few layered graphene nanosheets by 1-naphthol in water.

3.4 Adsorption at different pH values:

Investigation of adsorption capacity of adsorbents at different pH is important because of the presence of different ions in the wastewater which make it acidic or alkaline in nature. These conditions will greatly influence the nature of interactions between adsorbate and adsorbent and hence affects the efficiency between the adsorbent and adsorbate. Effect of pH on the adsorption of 1-naphthol on l-rGO is shown in Figure S5[§]. At lower and higher pH values, the adsorption capacity increases dramatically compared to that of the neutral condition. We assume the higher adsorption at lower pH values might be due to: (i) lower solubility of 1-naphthol in water at lower pH values (Table S3[§] shows that the solubility decreases slightly with decreasing pH), and due to (ii) the protonation of –OH groups of 1-naphthol which make the benzene ring an electron-depleted Lewis acid and induce strong interaction with the electron rich rGO surfaces acting as an electron-rich Lewis base, thus increasing the adsorption [9]. Similar to that of the acidic conditions, dramatic increase in the 1-naphthol adsorption is observed for alkaline conditions. It is reported that it might be due to the ionisation of the phenolic -OH group in 1-naphthol and thereby induced side reactions [9]. We believe that the strong adsorptive interaction between hydroxyl-substituted aromatics and rGO is mainly due to the electron-donating effect of the hydroxyl group due to the lone pair, which caused a strong electron-donor-acceptor (EDA) interaction between the adsorbates and the π-electron-depleted regions on the graphene surfaces of the rGO. Another type of EDA interaction is the π-π EDA interaction between the π-electron-rich aromatic ring(s) of the adsorbates and the π-electron-depleted regions on the rGO due to the defects. It is possible to have in the rGO, both electron-rich and -depleted sites, caused primarily by the surface defects [36].

4. Conclusions

In conclusion, rGO exhibits the highest adsorption efficiency for 1-naphthol compared to that of any adsorbents reported in the literature. At 303 K, q_{max} values of l-rGO and h-rGO are 3.57 and 5.55 mmol g^{-1}, respectively and at 323 K, the q_{max} of h-rGO for 1-naphthol is 8.6 mmol g^{-1}. This is the highest q_{max} value reported for 1-naphthol so far. The adsorption is endothermic in nature.

Acidic and alkaline pH increases the adsorption. The adsorption isotherms of the rGOs fit well with the Langmuir isotherm model. The higher and remarkable efficiency exhibited by rGO is assigned to the ability of 1-naphthol, to disperse rGO as few layered graphene nanosheets in water. AFM images confirm the exfoliation of rGO to nanosheets of 1-8 nm thickness by 1-naphthol.Our results point to the fact that modification of rGO to water dispersible graphene does not necessarily increase the adsorption efficiency, especially for compounds such as 1-naphthol and similar aromatic compounds, which are capable of dispersing rGO in aqueous solution. The result suggests that rGO can be dispersed in aqueous solution by naphthalene moieties having appropriate side groups. Our findings give a better understanding about the mechanism of adsorption of 1-naphthol by rGO. The results suggest that (non-modified) rGO is a super adsorbent for 1-naphthol and will probably be a very good adsorbent material for other aromatic compounds with structural similarities with 1-naphthol which can equally disperse rGO in water.

Notes and references

Department of Chemistry
Indian Institute of Space Science and Technology,
Thiruvananthapuram
Kerala 695 547, India
Email: sandhya@iist.ac.in

[§] Electronic Supplementary Information (ESI) available: [Details N$_2$ adsorption isotherm, effect of contact time on adsorption, effect of pH, digital photoimages& AFM images, kinetic fittings and parameters andsolubility at lower pH values are available]. See DOI: 10.1039/b000000x/

1. Zhang L, Li P, Gong Z and Li X. Photocatalytic degradation of polycyclic aromatic hydrocarbons on soil surfaces using TiO$_2$ under UV light. Journal of Hazardous Materials. 2008, 158, 478-484.
2. Taylor E, Cook B and Tarr M. Dissolved organic matter inhibition of sonochemical degradation of aqueous polycyclic aromatic hydrocarbons. Ultrasonics Sonochem.1999, 6, 175-183.
3. Raj A, Sander M, Janardhanan V and Kraft M. A study on the coagulation of polycyclic aromatic hydrocarbon clusters to determine their collision efficiency. Combustion and Flame 2010, 157, 523-534.
4. Barkay T, Navon-Venezia S, Ron E and Rosenberg E. Enhancement of Solubilization and Biodegradation of Polyaromatic Hydrocarbons by the Bioemulsifier Alasan. Applied and EnvironmentalMicrobiology. 1999, 65, 2697-2702.
5. Rafatullah M, Sulaiman O, Hashim R and Ahmad A. Adsorption of methylene blue on low-cost adsorbents: A review. Journal of Hazardous Materials. 2010, 177, 70-80.
6. Valderrama C, Gamisans X, de las Heras X, Farran A and Cortina J. Sorption kinetics of polycyclic aromatic hydrocarbons removal using granular activated carbon: Intraparticle diffusion coefficients. Journal of Hazardous Materials. 2008, 157, 386-396.
7. Walters R and Luthy R. Equilibrium adsorption of polycyclic aromatic hydrocarbons from water onto activated carbon.Environmental Science and Technology.1984, 18, 395-403.
8. Yang K, Zhu L and Xing B. Adsorption of Polycyclic Aromatic Hydrocarbons by Carbon Nanomaterials. Environmental Science and Technology.2006, 40, 1855- 1861.

9. Zhao G, Jiang L, He Y, Li J, Dong H, Wang X and Hu W. Sulfonated Graphene for Persistent Aromatic Pollutant Management. Advanced Materials. 2011, 23, 3959-3963.

10. Yang X, Chen C, Li J, Zhao G, Ren X and Wang X. Graphene oxide-iron oxide and reduced graphene oxide-iron oxide hybrid materials for the removal of organic and inorganic pollutants. RSC Advances. 2012, 2, 8821-8826.

11. Li Y, Zhang P, Du Q, Peng X, Liu T, Wang Z, Xia Y, Zhang W, Wang K, Zhu H and Wu D. Adsorption of fluoride from aqueous solution by graphene. Journal of Colloid and Interface Science. 2011, 363, 348-354.

12. Deng X, Lu L, Li W and Luo F. The adsorption properties of Pb(II) and Cd(II) on functionalized graphene prepared by electrolysis method. Journal of Hazardous Materials. 2010, 183, 923-930.

13. Zhu J, Wei S, Gu H, Rapole S, Wang Q, Luo Z, Haldolaarachchige N, Young D and Guo Z. One-pot synthesis of magnetic graphene nanocomposites decorated with core@double-shell nanoparticles for fast chromium removal. Environmental Science and Technology. 2012, 46, 977-985.

14. Liu T, Li Y, Du Q, Sun J, Jiao Y, Yang G, Wang Z, Xia Y, Zhang W, Wang K, Zhu H and Wu D. Adsorption of methylene blue from aqueous solution by graphene. Colloids and Surfaces B: Biointerfaces. 2012, 90, 197-203.

15. Ramesha G, Kumara A, Muralidhara H and Sampath S. Graphene and graphene oxide as effective adsorbents toward anionic and cationic dyes. Journal of Colloid and Interface Science. 2011, 361, 270-277.

16. Parvez K, Wu Z.S., Li R, Liu X, Graf R, Feng X and Mullen K. Exfoliation of Graphite into Graphene in Aqueous Solutions of Inorganic Salts. Journal of the American Chemical Society. 2014, 136, 6083-6091.

17. Gross M.A, Sales M.J, Soler M.A.G, Pereira-da-silva M.A, Da silva M.F.P and Paterno L.G. Reduced graphene oxide multilayers for gas and liquid phases chemical sensing. RSC advances. 2014, 4, 17917-17924.

18. Pei Z,Li L, Sun L, Zhan S, Shan X.Q, Yang S and Wen B. Adsorption characteristics of 1,2,4-trichlorobenzene, 2,4,6trichlorophenol, 2-naphthol and naphthalene on graphene and graphene oxide. Carbon. 2013, 51, 156-163.

19. Wang S, Sun H, Ang H.M and Tade M.O. Adsorptive remediation of environmental pollutants using novel graphene based nanomaterials. Chemical Engineering Journal. 2013, 226, 336-347.

20. Montes-Navajas P, Asenjo N.G, Santamaria R, Menedez R, Corma A and Garcia H. Surface Area Measurement of Graphene Oxide in Aqueous Solutions. Langmuir. 2013, 29, 13443-13448.

21. Zhao G, Li J and Wang X. Kinetic and thermodynamic study of 1-naphthol adsorption from aqueous solution to sulfonated graphene nanosheets. Chemical Engineering Journal. 2011, 173, 185-190.

22. Venugopal G, Krishnamoorthy K, Mohan R and Kim S.J. An investigation of the electrical transport properties of graphene-oxide thin films. Materials Chemistry and Physics. 2012, 132, 29-33.

23. Zhen Q, Hing Ip W, Lin X, Yousefi N, Yeung K.K, Li Z and Kim J.K. Transparent Conductive Films Consisting of Ultralarge Graphene Sheets Produced by Langmuir Blodgett Assembly. ACS nano. 2011, 5, 6039-6051.

24. Stankovich S, Dikin D, Piner R, Kohlhaas K, Kleinhammes A, Jia Y, Wu Y, Nguyen S.T and Ruoff R.S. Synthesis of graphene-based nanosheets via chemical reduction of exfoliated graphite oxide. Carbon 2007, 45, 1558-1565.

25. I. Langmuir, The adsorption of gases on plane surfaces of glass, mica and platinum, J. Am. Chem. Soc. 40 (1918) 1361–1403.

26. Xu J, Wang L and Zhu Y. Decontamination of Bisphenol A from Aqueous Solution by Graphene Adsorption. Langmuir. 28 (2012) 8418-8425.

27. Freundlich H.M.F. Uber die adsorption in losungen. Z. Phys. Chem. 57 (1906) 385–470

28. Weber T and Chakkravorti R. Pore and solid diffusion models for fixed bed adsorbers, AIChe Journal. 1974, 20, 228-238.

29. Hameed B.H, Din A.T.M and Ahmad A.L. Adsorption of methylene blue onto bamboo-based activated carbon: Kinetics and equilibrium studies. Journal of Hazardous Materials. 2007, 141, 819-825.

30. Sheng G.D, Shao D.D, Ren X.M, Wang X.Q, Li J.X, Chen Y.X and Wang X.K. Kinetics and thermodynamics of adsorption of ionizable aromatic compounds from aqueous solutions by as-prepared and oxidized multi-walled carbon nanotubes. Journal of Hazardous Materials. 2010, 178, 505-516.

31. Wei J, Zhu R, Zhu J, Ge F, Yuan P, He H and Ming C. Simultaneous sorption of crystal violet and 2-naphthol to bentonite with different CECs. Journal of Hazardous Materials. 2009, 166, 195-199.

32. Schlierf A, Yang H, Gebremedhn E, Treossi E, Ortolani L, Chen L, Minoia A, Morandi V, Samorì P, Casiraghi C, Beljonne D and Palermo V. Nanoscale insight into the exfoliation mechanism of graphene with organic dyes: effect of charge, dipole and molecular structure. Nanoscale. 2013, **5**, 4205-4216.

33. Parviz D, Das S, Ahmed T, Irin F, Bhattacharia S and Green M.J. Dispersions of Non-Covalently Functionalized Graphene with Minimal Stabilizer. ACS Nano. 2012, 6, 8857-8867.

34. Seo J.W.T, Green A.A, Antaris A.L and Hersam M.C. High-concentration aqueous dispersions of graphene using nonionic, biocompatible block copolymers. Journal of Physical Chemistry Letters. 2011, 2, 1004-1008.

35. Kim E.J, Xu J, Dang D.K, Tran V.T, Liu X, Chung J.S, Hur S.H, Choi W.M, and Kohl P.A. Liquid-phase exfoliation of graphene in organic solvents with additionof naphthalene. Journal of Colloid and Interface Science. 2014, 418, 37-42.

36. Chen W, Duan L, Wang L and Zhu D. Adsorption of hydroxyl- and amino-substituted aromatics to carbon nanotubes. Environmental Science and Technology. 2008, 42, 6862-6868.